ACS APPLIED ENERGY MATERIALS

www.acsaem.org Article

Inorganic Perovskite Solar Cells with High Voltage and Excellent Thermal and Environmental Stability

Junhao Zhu, Ranjith Kottokkaran, Saba Sharikadze, Harshavardhan Gaonkar, Laila-Parvin Poly, Arkadi Akopian, and Vikram L. Dalal*

Cite This: *ACS Appl. Energy Mater.* 2022, 5, 6265−6273 Read Online

ACCESS | Metrics & More | Article Recommendations | Supporting Information

ABSTRACT: The lack of high temperature and atmospheric stability of perovskite solar cells has been one of the primary obstacles hindering the commercialization of this emerging photovoltaic material. This work presents an all-inorganic $CsPbBr_3$ perovskite solar cell with excellent stability under both thermal and environmental stress. The perovskite layer was fabricated with a well-controlled layer-by-layer vapor deposition technique and subsequently annealed in a two-stage process. The solar cells have an overall device architecture of FTO/c-TiO_2/$CsPbBr_3$/buffer layer/P3HT/Au. A large band gap $PbBr_2$ buffer layer is inserted between the intrinsic layer and the hole transport layer. This layer inhibits the recombination of electrons at the p−i interface, improving the performance of the solar cell. The open-circuit voltage exhibited by these devices is 1.64 V, the highest open-circuit voltage (V_{oc}) ever reported for this perovskite material. Additionally, the devices yielded a photo-conversion efficiency of 7.9%. The isolated perovskite layer showed no degradation when annealed at temperatures up to 300 °C for 24 h. The solar cells withstood exposure to an environment of ambient air at 20 °C for 500 h without any loss in efficiency. Even a high-temperature (200 °C) exposure in air did not result in changes in the efficiency. The excellent environmental tolerance and high V_{oc} indicate the potential for this perovskite to be used in a 4-terminal tandem solar cell arrangement with Si.

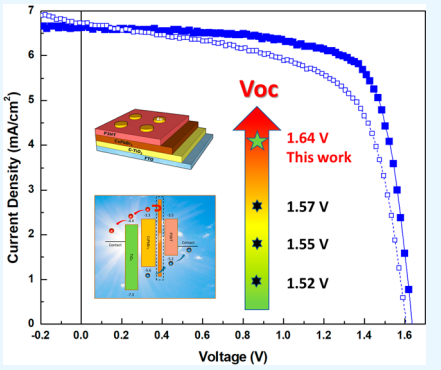

KEYWORDS: *inorganic perovskite solar cells, thermal stability, environmental stability, bromide perovskites, vacuum deposition, layer-by-layer deposition*

INTRODUCTION

The perovskite solar cell (PSC) is an important technology for next-generation solar energy conversion. PSCs have attracted significant attention in the renewable energy conversion device field due to the promising electro-optical properties such as high absorption coefficient and long carrier diffusion length. Since the introduction of PSCs in 2009, a great deal of global effort has been devoted to perovskite materials, which has resulted in a dramatic increase in the photo conversion efficiency to 25.2%.[1−10] Despite the decade of excellent improvement in the efficiency, thermal and moisture instability still pose potentially fatal flaws for PSCs and need to be further addressed if true commercial viability is to be achieved.[11−14]

It is well known that either organic or hybrid inorganic−organic perovskite solar cells decompose at relatively low temperatures less than 100 °C.[15,16] Consequently, such devices are marginally useful in hot, desert environments where the cell temperature often reaches 90−100 °C.[17−19] Our previous work shows that excellent thermal stability at 200 °C for long period of time is achievable through use of all-inorganic perovskite materials comprising CsPb(I,Br) alloys.[20] However, such inorganic perovskite materials proved to be unstable when exposed to moisture. Solar cell device degradation occurred even during short duration electrical characterization performed in air. The ambient environment device degradation is particularly acute when PSCs are made using a high I/Br ratio.[21] In this report, all-brominated, iodine-free, $CsPbBr_3$ perovskite materials and solar cell devices are investigated. We find that the materials and devices exhibit excellent thermal and environmental stability.

$CsPbBr_3$ is a wide band gap (~2.3 eV) semiconductor, which is of significant importance for making tandem junction cells. The use of this material with another perovskite device as the bottom cell is especially important for the creation of entirely thin-film tandem devices.[22] Theoretically, higher V_{oc} should be expected for such a wide band gap light harvester and is also desired for improving the all-brominated device efficiency. Till date, the highest V_{oc} of thermally prepared $CsPbBr_3$ perovskite cell has stagnated around 1.5 V, resulting

Received: February 27, 2022
Accepted: April 12, 2022
Published: April 20, 2022

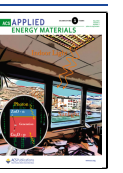

https://doi.org/10.1021/acsaem.2c00624
ACS Appl. Energy Mater. 2022, 5, 6265−6273

in much lower efficiency than solution-processed devices.[23−27] In 2018, Tang's group achieved 1.57 V V_{oc} on the solution-prepared $CsPbBr_3$ perovskite solar cell.[25] By utilizing a mixture of solution process and vapor deposition approach, Yang's group demonstrated 1.52 V V_{oc} in 2019.[36] Recently in 2022, Cheng's group achieved 1.55 V V_{oc} with pure physical vapor deposition (PVD) technique in this material.[32] Nevertheless, the solution growth technique generally has inherent problems with reproducibility and scalability. On the other hand, the vapor-based process allows for precise control of growth parameters such as precursor ratio, substrate temperature, and film thickness. It is more industry-friendly in the sense of yield enhancement.

In this work, by optimizing the fabrication process and interface engineering, an outstanding 1.64 V open-circuit voltage was achieved with $CsPbBr_3$ solar cell devices. This is the highest ever reported open-circuit voltage in this perovskite material. Moreover, the excellent stability of this material and the solar cell device under ambient and thermal stress are systematically assessed in this report.

EXPERIMENTAL SECTION

All-bromine inorganic $CsPbBr_3$ PSC devices were fabricated with a n−i−p superstrate architecture (light is shining from the bottom n-layer) with the structure fluorine doped tin oxide (FTO)/compact-TiO_2/$CsPbBr_3$/P3HT/Au, as shown schematically in Figure 1.

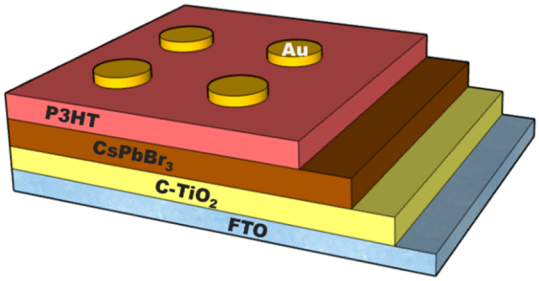

Figure 1. Schematic diagram of the superstrate n−i−p inorganic perovskite solar cell.

FTO-coated glass was first cleaned by sonication and boiling in 5% surfactant solution, DI water, methanol, acetone, and isopropanol for 20 min each. 10 min air plasma treatment was conducted before n-layer growth. The compact TiO_2 layer was prepared by following steps: (1) A solution of 0.5 M titanium isopropoxide and 0.5 M diethanolamine dissolved in ethanol was stirred and mixed at room temperature; (2) prepared solution was spin-coated to the FTO glass substrate at 7000 RPM and dried on a hot plate to get rid of extra solution; and the (3) prepared film was then sintered at 500 °C for 2 h.

The perovskite film was grown using well-controlled evaporation from multiple source boats within Luxel Radak furnaces, as shown in Figure 2. One boat held $PbBr_2$ powder, and the other boat held CsBr powder. The $CsPbBr_3$ film was deposited using a sequential evaporation technique where a thick layer of one material was grown followed by the growth of the other material. The best device performance was achieved when the perovskite material was composed of three constituent layers, with CsBr as bottom and top layers and $PbBr_2$ in the center (CsBr/$PbBr_2$/CsBr). Optimized perovskite film thickness was obtained using 136 nm for each layer of the CsBr and 377 nm for the $PbBr_2$ layer, resulting in a total thickness of 650 nm perovskite material. The substrate was held at 200 °C during the deposition process. After the thermal evaporation, the films were subjected to annealing under various conditions.

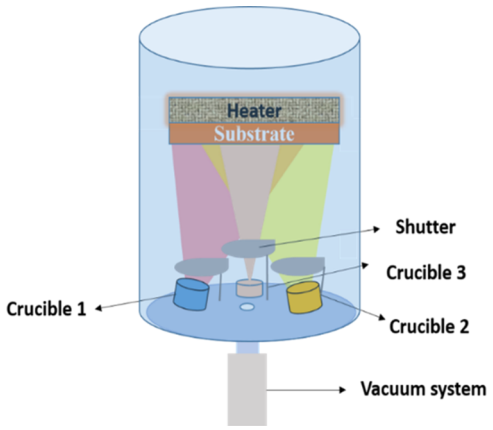

Figure 2. Schematic of the homemade vacuum thermal evaporator where $CsPbBr_3$ perovskite thin films were deposited.

Poly(3-hexylthiophene-2,5-diyl) (P3HT) was used as the hole transport p-layer. 15 mg/mL in chlorobenzene solution was prepared and spin-coated on the annealed perovskite film at 2000 RPM for 60 s in a nitrogen glovebox, followed by a 10 min hot plate annealing at 150 °C. The gold top contact was evaporated on the very top to finish the fabrication of the PSC device. A circular shadow mask was used to define 0.106 cm^2 active contact area for the solar cells.

An ABET full-spectrum AM1.5 solar simulator was used to measure the electrical performance of each solar cell inside and outside of the nitrogen environment glove box. A standard silicon reference cell from Pacific Sensors was used for the calibration of the solar simulator. $J-V$ curves were measured by scanning voltage and measuring current controlled by a Lab-View-based program. The quantum efficiency (QE) and subgap QE were measured using a custom-built system with a chopped monochromatic light source, optical filters, and lock-in amplifiers synchronized to the chopped source. X-ray diffraction (XRD) was measured using a Rigaku Ultima X-ray diffractometer with a Cu Kα radiation source (λ = 1.54 A) at 44 kV and 40 mA. Scanning electron microscope images were taken by a FEI Quanta 250 FE-SEM.

RESULTS AND DISCUSSION

Device Properties. For a wide band gap semiconductor material with ∼2.3 eV gap, a high voltage for the solar cell device is highly desired to approach the theoretical possible efficiency. However, our preliminary data showed that the $CsPbBr_3$ PSC devices we made have open-circuit voltage only around 1.4 V, which indicated almost 1 V voltage loss of the device. Referring to the work by the Cohen group,[28] the voltage loss mechanism for a perovskite solar device has two main root causes aside from the thermodynamic limits and non-radiative recombination: (a) energy band misalignment and (b) poor interfaces between the intrinsic layer and the n and p heterojunctions. It is not easy to find proper transport layer materials whose band diagrams perfectly match with $CsPbBr_3$.[29−31,33] In this study, we focus on the strategy to improve $CsPbBr_3$/transport layer interfaces.

A previous study has shown that a two-stage annealing process can effectively modify the $CsPbBr_3$ morphologies and reduce the defect densities.[32] A similar two-step annealing process was adopted and optimized in this work with a higher temperature, short duration anneal followed by a lower temperature, high duration anneal. Figure 3 shows the SEM images of the $CsPbBr_3$ film surface after being annealed at three different conditions: 320 °C/20 min + 300 °C/40 min, 400 °C/20 min + 350 °C/40 min, and 450 °C/20 min + 350 °C/40 min. A significant increase in the grain size can be found

https://doi.org/10.1021/acsaem.2c00624
ACS Appl. Energy Mater. 2022, 5, 6265−6273

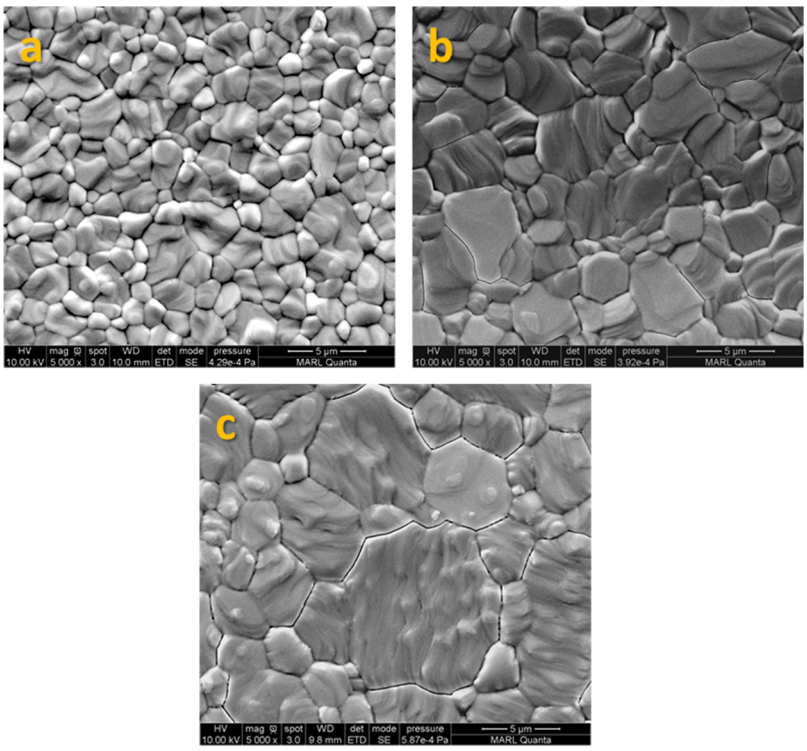

Figure 3. SEM images of perovskite annealed at two-step temperatures: (a) 320 °C/20 min + 300 °C/40 min; (b) 400 °C/20 min + 350 °C/40 min; and (c) 450 °C/20 min + 350 °C/40 min.

as a function of increasing annealing temperatures. About 10 μm large grain was obtained when the film was annealed at 450 °C and 350 °C conditions. Using 450 °C as the high-temperature annealing condition provides the initial energy for a better reaction of CsBr and $PbBr_2$ films that were individually evaporated onto the substrate. The following lower temperature, longer duration sintering process is beneficial for the formed $CsPbBr_3$ perovskite structure to become fully crystallized and results in extensive growth of the grains. The corresponding XRD spectrum is in good agreement with the SEM results, as shown in Figure 4. Two major intensity peaks located at 2θ = 15.2 and 30.8° were found on each two-step annealed $CsPbBr_3$ films, which were assigned to (1 0 0) and (2 0 0) planes of the cubic $CsPbBr_3$ phase ($Pm3m$).[32] Almost none of other CsBr- or $PbBr_2$-rich phases were exhibited in the XRD pattern, indicating high perovskite crystallinity achieved by the sequential deposition technique and subsequent two-step annealing process. Heightened intensity of both two peaks was obtained as the annealing temperature increases, which is congruent with what has been found in SEM images. From these test results, we deduce that complete crystallization and extensive grain growth were achieved. Film degradation begins to occur at annealing temperatures surpassing 450 °C.

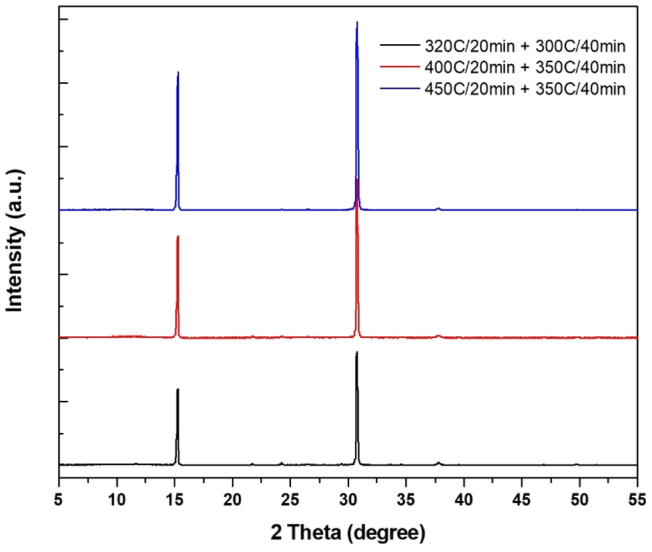

Figure 4. XRD of $CsPbBr_3$ films annealed at different two-stage temperature profiles.

The $CsPbBr_3$ solar cell device photovoltaic performance (J–V) with corresponding annealing conditions is shown in Figure 5. When the device was not annealed at high enough temperatures (*e.g.*, 320 °C/20 min + 300 °C/40 min), the open-circuit voltage (V_{oc}) of the cell was only 1.37 V. Higher annealing temperatures (450 °C/20 min + 350 °C/40 min) help in enhancing the grain growth and crystallization, resulting in higher V_{oc} of 1.54 V. Larger grains and higher crystallinity usually lead to reduced defect densities in the film, thereby reducing the voltage loss from this 2.3 eV wide material. The assumption of reduced grain boundary defects is also supported by the J–V curves, in which the higher-temperature annealing cycle results in increased short-circuit current (J_{sc}).

Further optimization of the device was carried out by changing the interface of the perovskite and p-type hole transport layer (HTL). We deposited an extra $PbBr_2$ cap layer at the end of the deposition after high-temperature annealing cycle. The device was further annealed at 300 °C/15 min after the deposition of the buffer layer. Figure 6 shows the band diagram of the FTO/compact-TiO_2/$CsPbBr_3$/P3HT/Au solar cell device. By adding a thin layer of $PbBr_2$, which is a ~4.2 eV

https://doi.org/10.1021/acsaem.2c00624
ACS Appl. Energy Mater. 2022, 5, 6265−6273

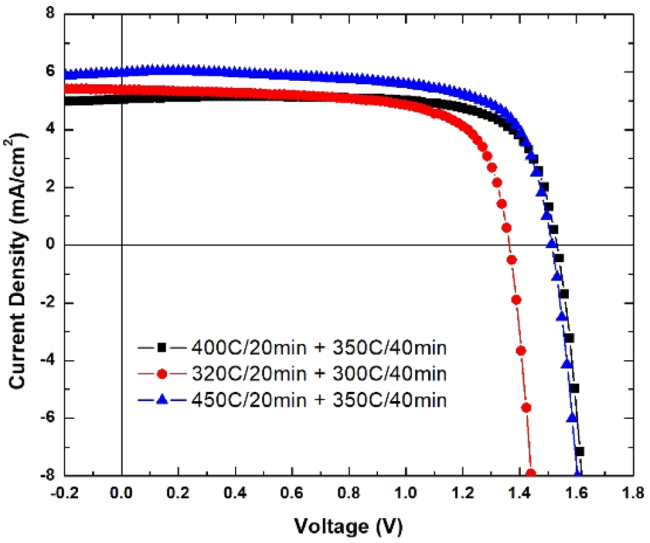

Figure 5. $J-V$ curves showing the influence of different temperatures of the two-step annealing profile on the solar cell device performance.

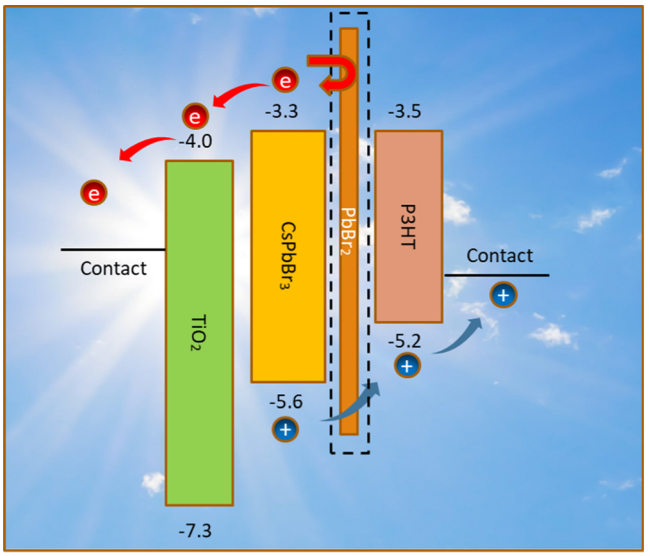

Figure 6. Band diagram of the FTO/compact-TiO_2/$CsPbBr_3$/P3HT/Au solar cell device with an extra thin $PbBr_2$ cap layer added.

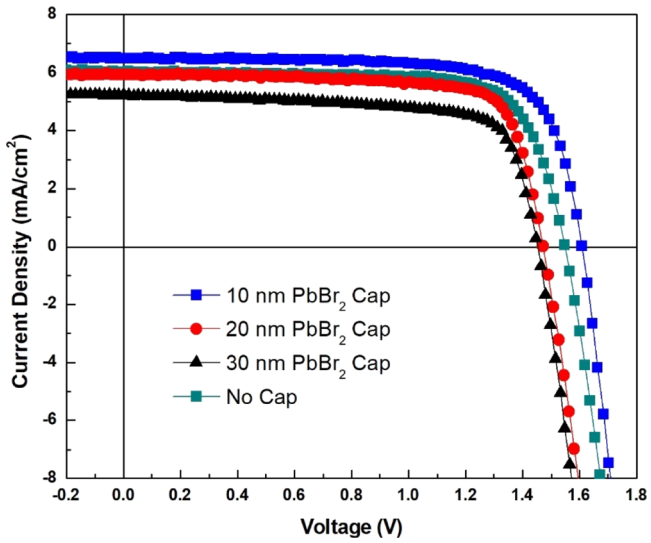

Figure 7. $J-V$ performance of the solar cell device with differing $PbBr_2$ cap layer thicknesses.

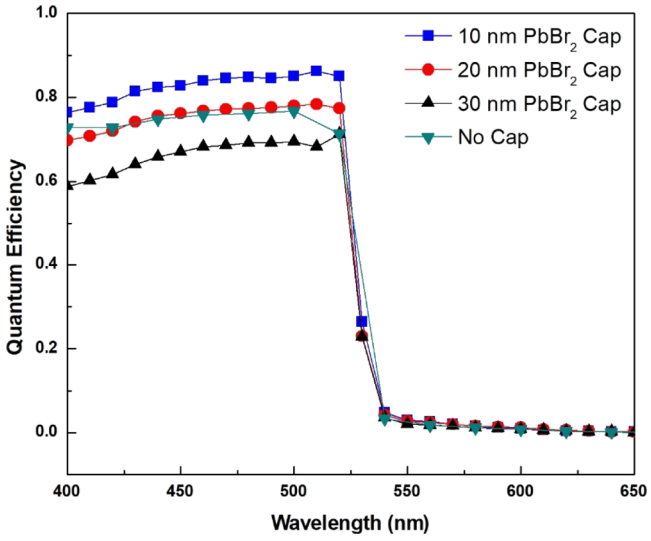

Figure 8. QE performance of the solar cell device with differing $PbBr_2$ cap layer thicknesses.

wide band gap material,[35] a potential step is created at the p−i interface. The E_c energy difference creates a significantly higher barrier for electron flow than what exists at the P3HT/perovskite interface (see Figure 6), thereby reducing the electron recombination at that interface. Optimization of the $PbBr_2$ cap layer thickness is crucial for enacting the theory without incurring negative consequences. If the additional $PbBr_2$ layer is too thick, then the hold transport at the interface may become impeded.

Results from $PbBr_2$ cap layer thicknesses of 10, 20 and 30 nm are given in this report. Figure 7 shows the $J-V$ curve of the device with different cap layer thicknesses. There is a clear trend in the data. A 10 nm thick $PbBr_2$ helped boost the J_{sc} up to 6.5 mA/cm^2 when compared with the control group (no cap) which is 6.0 mA/cm^2. Upon increasing the cap layer thickness to 20 and 30 nm, short-circuit current density decreases to values lower than the control group. More clarity about this phenomenon is provided by the QE measurement, as shown in Figure 8. Initially, the thin cap layer improves the QE, particularly for long wavelengths (520 nm) from the reduction in electron recombination at this interface. As we increase the thickness of the cap layer, the QE begins to decrease at all wavelengths. This is attributed to the necessity of tunneling for holes to travel through the $PbBr_2$ barrier layer. The efficiency of tunneling across this layer decreases as a function of thickness. Further increase to 30 nm suppresses the tunneling even more. The apparent resistance indicated by the slope of the $J-V$ curve at V_{oc} also increases as the thickness of the barrier layer increases, further supporting the hypothesis that a thick layer impedes the transport of holes. Thus, we have shown that an appropriate thickness of a buffer layer at the p−i interface improves the device.

In Table 1 below, we show the values of various photovoltaic parameters as a function of the thickness of the $PbBr_2$ layer.

Noticeably, from Table 1 and Figure 7, the open-circuit voltage also increased slightly as we insert a 10 nm $PbBr_2$ cap layer into the device. An added advantage of $PbBr_2$, an inactive material in air, is that it encapsulates the $CsPbBr_3$ perovskite

https://doi.org/10.1021/acsaem.2c00624
ACS Appl. Energy Mater. 2022, 5, 6265−6273

Table 1. Specific Parameters of the $CsPbBr_3$ Solar Cell with Various $PbBr_2$ Cap Layer Thicknesses

device	V_{oc} (V)	J_{sc} (mA/cm^2)	FF (%)	PCE (%)
no cap	1.55	6.02	73	6.8
10 nm $PbBr_2$ cap	1.62	6.50	73	7.7
20 nm $PbBr_2$ cap	1.48	5.94	74	6.5
30 nm $PbBr_2$ cap	1.45	5.22	73	5.5

surface and bolsters the device resistance to moisture. Using all the process optimization techniques described in this work, we have manifested a V_{oc} of 1.64 V with 7.9% energy conversion efficiency. Figure 9 shows the $J-V$ curve and QE of the

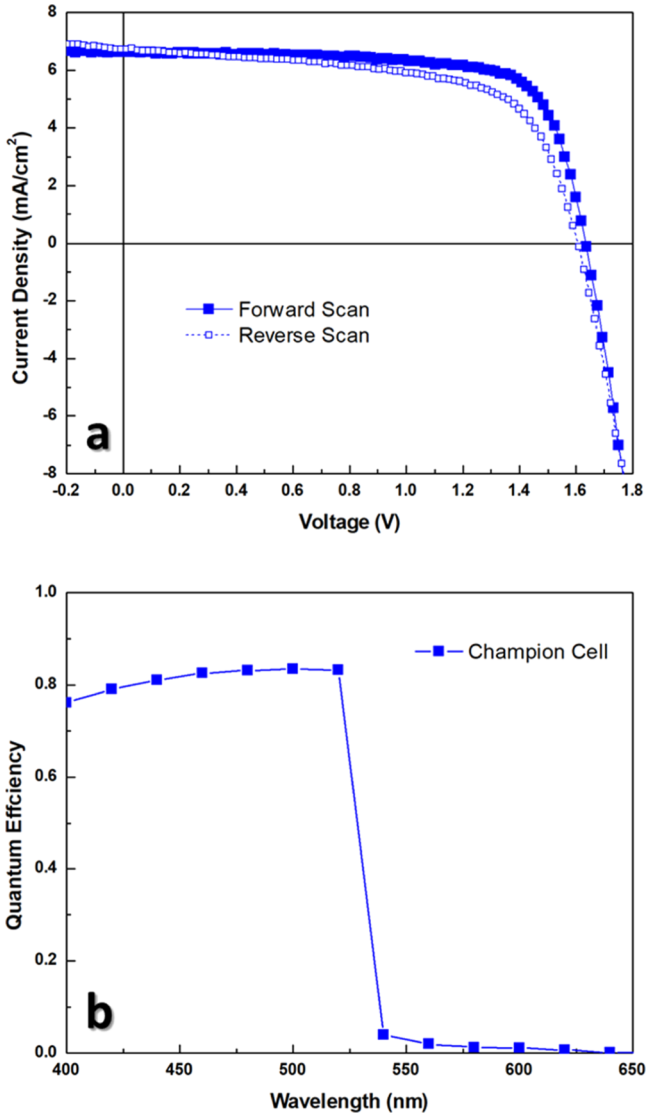

Figure 9. With extra 10 nm of $PbBr_2$ after annealing, 7.9% solar cell with ultrahigh 1.64 V voltage has been achieved. (a) $J-V$ curve with forward and reverse scan (b) QE for the champion cell.

champion cell, with the detailed device performance parameter listed in Table 2. In Figure 10, we show the histogram for six cells, showing excellent repeatability in the performance.

Stability. Thermal and environmental degradation is a well-known problem of perovskite solar cell devices. This is one of the main focuses of our research and will be addressed in this work. As demonstrated by our previous work with mixed

Table 2. Specific Parameters of the $CsPbBr_3$ Champion Cell Performance

device	V_{oc} (V)	J_{sc} (mA/cm^2)	FF (%)	PCE (%)
champion cell	1.64	6.72	71	7.9

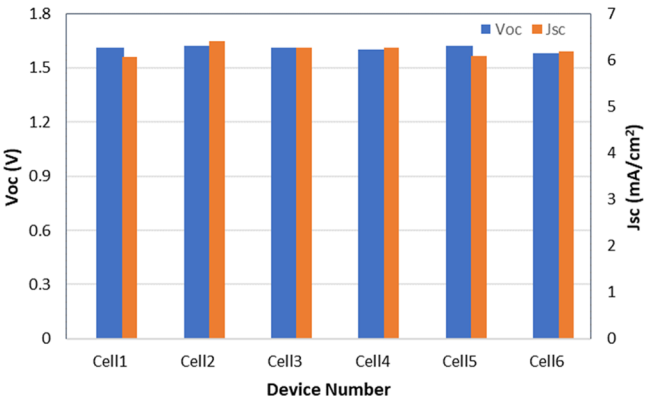

Figure 10. Histogram of V_{oc} and J_{sc} for repeated solar cell devices.

halide perovskite material $CsPbI_2Br$, great thermal stability was validated with such cells. However, all the fabrication and characterization work were restricted inside a N_2 glovebox as the cell would degrade dramatically with exposure to the air. As mentioned, the elimination of the iodine content from the perovskite should result in a device with better stability under both thermal and environmental stress.

After fabrication, the $CsPbBr_3$ PSC device was exposed to the ambient air (20 °C and relative humidity 40%) for over 500 h. Figure 11 shows the device efficiency change over 100 h

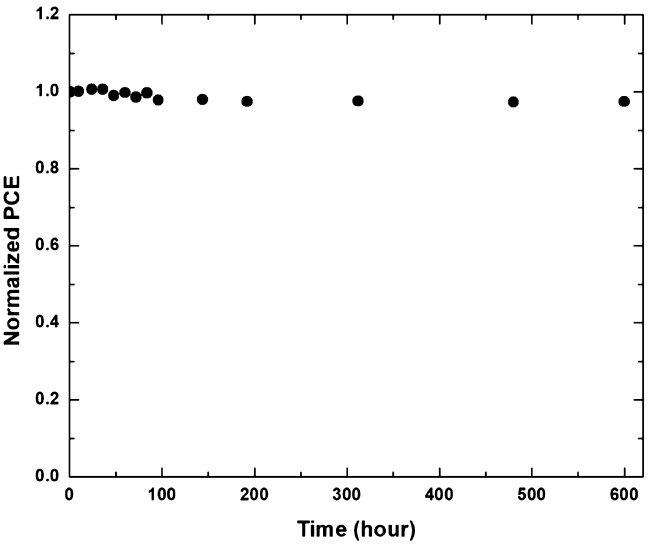

Figure 11. Normalized PCE of the $CsPbBr_3$ perovskite solar cell exposed in ambient air. The device efficiency shows only about 2% change over 500 h exposure.

normalized to the initial measured value immediately after fabrication. Virtually no degradation of the cell efficiency has been observed. This result was confirmed by the comparison of the device $J-V$ characteristic after continuous air exposure for 25 days, as shown in Figure 12. After over 500 h, the $J-V$ curve for the cell was almost identical to the initial $J-V$ curve, which

https://doi.org/10.1021/acsaem.2c00624
ACS Appl. Energy Mater. 2022, 5, 6265−6273

demonstrated promising robustness of the device under the moisture stress.

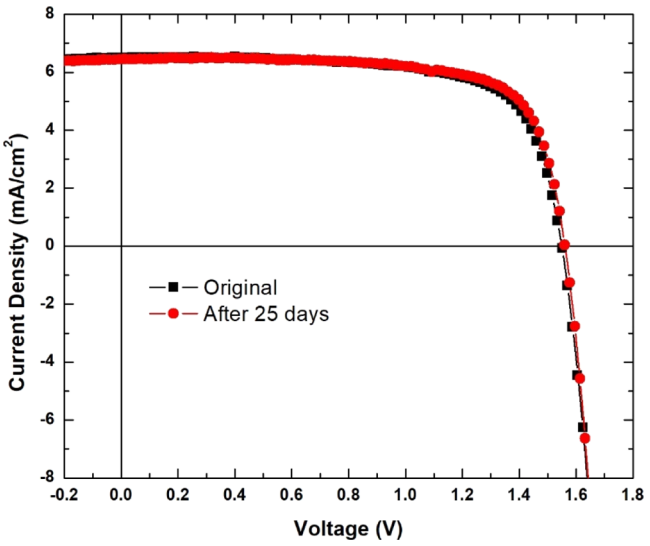

Figure 12. $J-V$ curve of the device performance shows no change over 25 days exposure in ambient air.

We next studied the stability of the cell under both thermal and ambient stress. Figure 13 shows the XRD data for

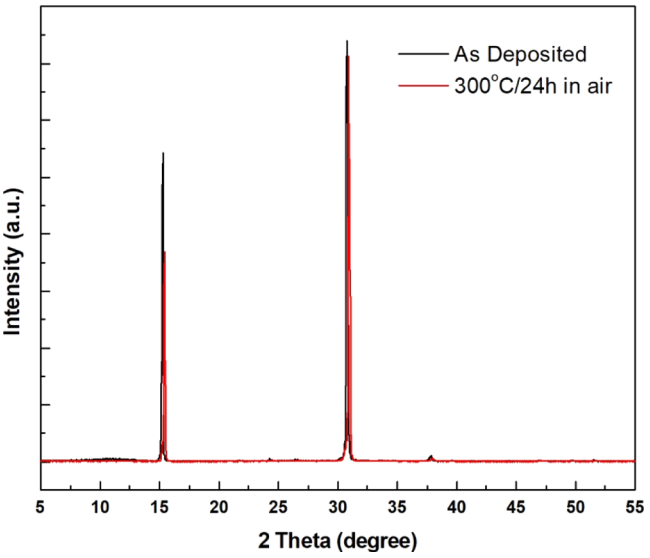

Figure 13. XRD patterns for $CsPbBr_3$ perovskite films before and after annealing at 300 °C for 24 h in ambient air.

perovskite material itself under the high-temperature stress test in the ambient air environment. The $CsPbBr_3$ film was deposited on the glass slide and heated at 300 °C for 24 h in air. It is well known that an unstable perovskite decomposed into a Pb phase (*e.g.*, PbI_2 or $PbBr_2$) upon heating. This behavior can be easily picked up in the X-ray spectrum. Compared the XRD data with the initial as-deposited spectrum, no decomposition of the all-brominated perovskite material was observed after being heated in the air. The intensity of (100) and (200) planes is comparable for measurements done before and after the environmental stress test detailed above. Additionally, there is no emergence of any new peaks on the post air anneal XRD spectrum. These results indicate that there is no degradation of the crystallinity of the perovskite material. This is a remarkable result and attests to the potential for the use of such materials as a stable, large band gap solar cell partner with Si or other perovskite in a four-terminal tandem cell arrangement.

The $CsPbBr_3$ solar cell device was also tested under similar thermal and ambient stress. Figure 14 shows the device

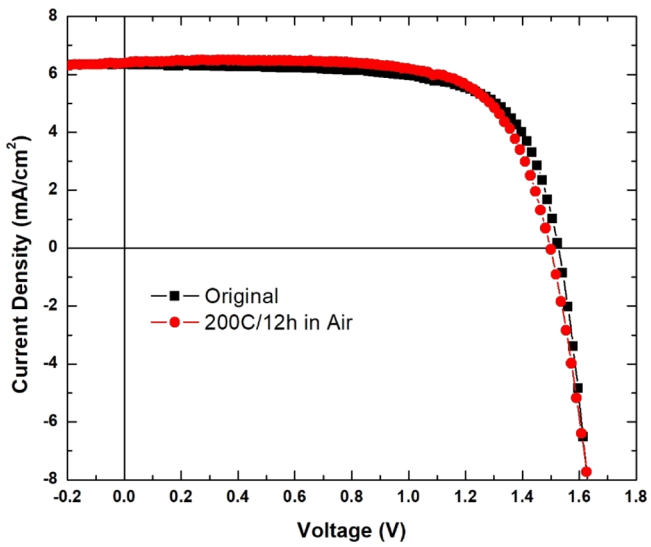

Figure 14. $J-V$ curve of the perovskite device for air stability at the high-temperature test.

performance ($J-V$ and QE curves) after heating the device at 200 °C for 12 h in the atmosphere. Both $J-V$ and QE curves showed no degradation of the device performance under such a stress test, indicating that the brominated perovskite solar cells are very stable and robust in real-world environments even at elevated temperatures.

Fundamental Material Properties. Fundamental material properties of the vacuum-deposited $CsPbBr_3$ perovskite films were also measured in this work. As a direct band gap material, the absorption coefficient is dependent to the source light photon energy following the equation

$$(\alpha h\nu)^2 = A(h\nu - E_g) \quad (1)$$

At long wavelengths, where α is small, the absorption is proportional to αt, where t is the thickness. Hence, one can plot external quantum efficiency (EQE), which is proportional to αt, instead of α in eq 1, to obtain the band gap. The result for the Tauc plot as $(\mathrm{EQE} \times E_{ph})^2$ *versus* E_{ph} in the cutoff region is shown in Figure 15. A linear intercept on the x-axis shows a band gap of 2.30 eV.

We also measured the subgap QE against the photon energy to determine the value of Urbach energy of the valence band tails. Urbach energy is an important parameter and impacts the open-circuit voltage of the solar cell.[34] A high value for Urbach energy indicates that tail state defects are extending far into the gap and will limit the movement of quasi-Fermi levels upon illumination, and therefore, limit the open-circuit voltage. A value of 22 meV for Urbach energy of valence band tails is obtained from Figure 16, which is in the usual range observed in all device-quality perovskite materials.

We also measured the $C-V$ curve of the device to determine the donor and shallow defect and built-in voltage. The data for

https://doi.org/10.1021/acsaem.2c00624
ACS Appl. Energy Mater. 2022, 5, 6265−6273

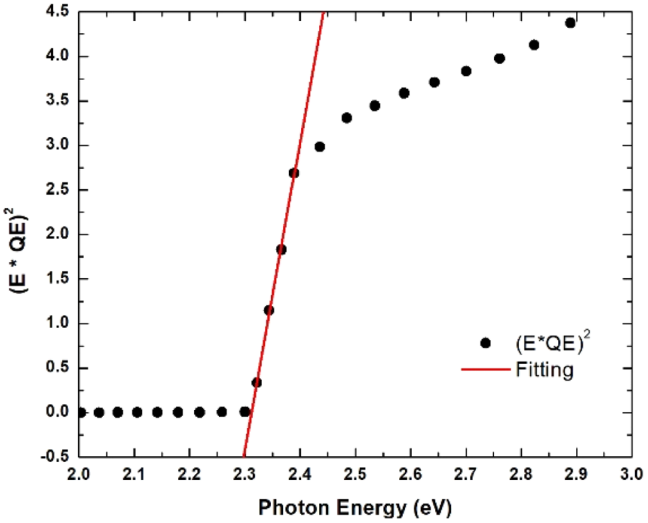

Figure 15. Tauc plot: (EQE × E_{ph})^2 plotted *vs* E_{ph} to determine the band gap of $CsPbBr_3$ perovskite material.

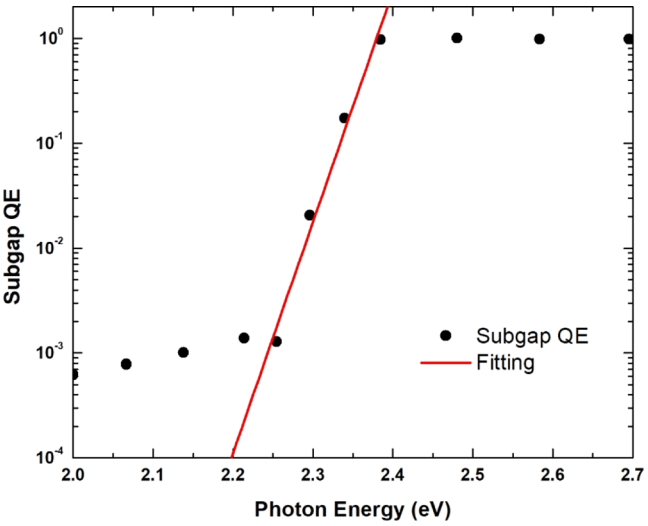

Figure 16. Sub-band gap absorption *vs* E_{ph} plotted to calculate the Urbach energy of tail states.

$1/C^2$ versus V curve are shown in Figure 17, which shows a defect density of 2.4 × 10^{15}/cm^3 and 1.61 V for the built-in voltage.

CONCLUSIONS

In summary, we have developed a solar cell device utilizing the all-inorganic, all-bromide perovskite material, $CsPbBr_3$, which exhibits very good stability under both thermal and ambient stress. The perovskite material itself shows no compositional degradation at 300 °C for 24 h in the air. Furthermore, $CsPbBr_3$ solar cell devices were demonstrated to have robust environmental stability with no performance degradation at 200 °C in the air for 12 h and show little efficiency loss after 500 h exposure in the ambient environment. We also show that the insertion of a thin, larger band gap capping layer at the p−i interface improves the device performance by reducing the electron recombination at this interface. By precise control of vacuum deposition processing and interface engineering, we have obtained the highest open-circuit voltage ever achieved, 1.64 V, in this perovskite material. The combination of

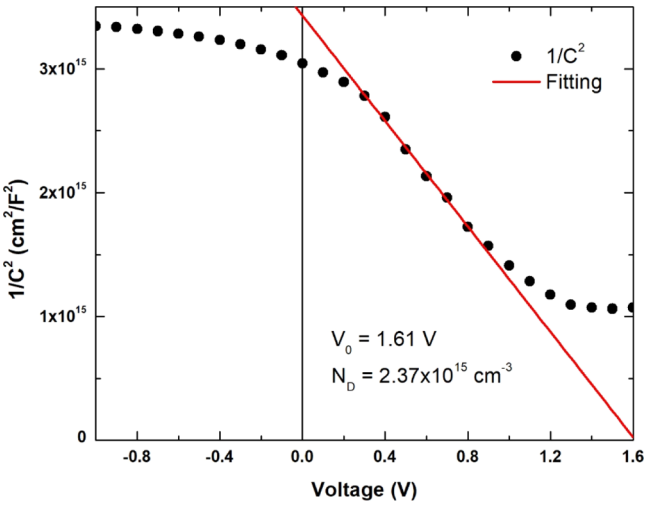

Figure 17. *C*−*V* plot to determine the built-in voltage V_0 and defect density of the $CsPbBr_3$ perovskite solar cell device.

excellent stability in the real-world environment at elevated temperatures, a high open-circuit voltage, and a very well-controlled processing technique indicates a significant potential for this material to be utilized in a four-terminal tandem cell system.

ASSOCIATED CONTENT

Supporting Information

The Supporting Information is available free of charge at https://pubs.acs.org/doi/10.1021/acsaem.2c00624.

Thickness measurement data of the as-deposited and annealed perovskite films (PDF)

AUTHOR INFORMATION

Corresponding Author

Vikram L. Dalal − *Department of Electrical and Computer Engineering, Iowa State University, Ames, Iowa 50010, United States; Microelectronics Research Center, Iowa State University, Ames, Iowa 50010, United States*; Email: vdalal@iastate.edu

Authors

Junhao Zhu − *Department of Electrical and Computer Engineering, Iowa State University, Ames, Iowa 50010, United States; Microelectronics Research Center, Iowa State University, Ames, Iowa 50010, United States*

Ranjith Kottokkaran − *Microelectronics Research Center, Iowa State University, Ames, Iowa 50010, United States*; orcid.org/0000-0001-5542-2719

Saba Sharikadze − *Department of Electrical and Computer Engineering, Iowa State University, Ames, Iowa 50010, United States; Microelectronics Research Center, Iowa State University, Ames, Iowa 50010, United States*

Harshavardhan Gaonkar − *Department of Electrical and Computer Engineering, Iowa State University, Ames, Iowa 50010, United States; Microelectronics Research Center, Iowa State University, Ames, Iowa 50010, United States*

Laila-Parvin Poly − *Department of Electrical and Computer Engineering, Iowa State University, Ames, Iowa 50010, United States; Microelectronics Research Center, Iowa State University, Ames, Iowa 50010, United States*

https://doi.org/10.1021/acsaem.2c00624
ACS Appl. Energy Mater. 2022, 5, 6265−6273

Arkadi Akopian − *Department of Electrical and Computer Engineering, Iowa State University, Ames, Iowa 50010, United States; Microelectronics Research Center, Iowa State University, Ames, Iowa 50010, United States*

Complete contact information is available at: https://pubs.acs.org/10.1021/acsaem.2c00624

Author Contributions

The manuscript was written through contributions of all authors. All authors have given approval to the final version of the manuscript.

Notes

The authors declare no competing financial interest.

■ ACKNOWLEDGMENTS

This work was supported in part by a grant from the National Science Foundation (EAGER-2035240). We also thank Max Noack for his technical help.

■ REFERENCES

(1) Jeon, N. J.; Na, H.; Jung, E. H.; Yang, T.-Y.; Lee, Y. G.; Kim, G.; Shin, H.-W.; Il Seok, S.; Lee, J.; Seo, J. A Fluorene-Terminated Hole-Transporting Material for Highly Efficient and Stable Perovskite Solar Cells. *Nat. Energy* **2018**, *3*, 682−689.

(2) Ye, Q.; Zhao, Y.; Mu, S.; Ma, F.; Gao, F.; Chu, Z.; Yin, Z.; Gao, P.; Zhang, X.; You, J. Cesium Lead Inorganic Solar Cell with Efficiency beyond 18% via Reduced Charge Recombination. *Adv. Mater.* **2019**, *31*, 1905143.

(3) Yan, L.; Xue, Q.; Liu, M.; Zhu, Z.; Tian, J.; Li, Z.; Chen, Z.; Chen, Z.; Yan, H.; Yip, H. L.; Cao, Y. Interface Engineering for All-Inorganic CsPbI 2 Br Perovskite Solar Cells with Efficiency over 14%. *Adv. Mater.* **2018**, *30*, 1802509.

(4) Chen, M.; Ju, M.-G.; Garces, H. F.; Carl, A. D.; Ono, L. K.; Hawash, Z.; Zhang, Y.; Shen, T.; Qi, Y.; Grimm, R. L.; Pacifici, D.; Zeng, X. C.; Zhou, Y.; Padture, N. P. Highly Stable and Efficient All-Inorganic Lead-Free Perovskite Solar Cells with Native-Oxide Passivation. *Nat. Commun.* **2019**, *10*, 16.

(5) Tian, J.; Xue, Q.; Tang, X.; Chen, Y.; Li, N.; Hu, Z.; Shi, T.; Wang, X.; Huang, F.; Brabec, C. J.; Yip, H. L.; Cao, Y. Dual Interfacial Design for Efficient CsPbI 2 Br Perovskite Solar Cells with Improved Photostability. *Adv. Mater.* **2019**, *31*, 1901152.

(6) Saliba, M.; Matsui, T.; Domanski, K.; Seo, J.-Y.; Ummadisingu, A.; Zakeeruddin, S. M.; Correa-Baena, J.-P.; Tress, W. R.; Abate, A.; Hagfeldt, A.; Grätzel, M. Incorporation of Rubidium Cations into Perovskite Solar Cells Improves Photovoltaic Performance. *Science* **2016**, *354*, 206.

(7) Correa-Baena, J.-P.; Luo, Y.; Brenner, T. M.; Snaider, J.; Sun, S.; Li, X.; Jensen, M. A.; Hartono, N. T. P.; Nienhaus, L.; Wieghold, S.; Poindexter, J. R.; Wang, S.; Meng, Y. S.; Wang, T.; Lai, B.; Holt, M. V.; Cai, Z.; Bawendi, M. G.; Huang, L.; Buonassisi, T.; Fenning, D. P. Homogenized Halides and Alkali Cation Segregation in Alloyed Organic-Inorganic Perovskites. *Science* **2019**, *363*, 627−631.

(8) Song, T.-B.; Chen, Q.; Zhou, H.; Jiang, C.; Wang, H.-H.; Yang, Y.; Liu, Y.; You, J.; Yang, Y. Perovskite Solar Cells: Film Formation and Properties. *J. Mater. Chem. A* **2015**, *3*, 9032−9050.

(9) Liu, M.; Johnston, M. B.; Snaith, H. J. Efficient Planar Heterojunction Perovskite Solar Cells by Vapour Deposition. *Nature* **2013**, *501*, 395−398.

(10) Park, N.-G. Perovskite Solar Cells: An Emerging Photovoltaic Technology. *Mater. Today* **2015**, *18*, 65−72.

(11) Meng, L.; You, J.; Yang, Y. Addressing the Stability Issue of Perovskite Solar Cells for Commercial Applications. *Nat. Commun.* **2018**, *9*, 5265.

(12) Zeng, Q.; Zhang, X.; Feng, X.; Lu, S.; Chen, Z.; Yong, X.; Redfern, S. A. T.; Wei, H.; Wang, H.; Shen, H.; Zhang, W.; Zheng, W.; Zhang, H.; Tse, J. S.; Yang, B. Polymer-Passivated Inorganic Cesium Lead Mixed-Halide Perovskites for Stable and Efficient Solar Cells with High Open-Circuit Voltage over 1.3 V. *Adv. Mater.* **2018**, *30*, 1705393.

(13) Nam, J. K.; Chai, S. U.; Cha, W.; Choi, Y. J.; Kim, W.; Jung, M. S.; Kwon, J.; Kim, D.; Park, J. H. Potassium Incorporation for Enhanced Performance and Stability of Fully Inorganic Cesium Lead Halide Perovskite Solar Cells. *Nano Lett.* **2017**, *17*, 2028−2033.

(14) Myung, C. W.; Yun, J.; Lee, G.; Kim, K. S. A New Perspective on the Role of A-Site Cations in Perovskite Solar Cells. *Adv. Energy Mater.* **2018**, *8*, 1702898.

(15) Abbas, H. A.; Kottokkaran, R.; Ganapathy, B.; Samiee, M.; Zhang, L.; Kitahara, A.; Noack, M.; Dalal, V. L. High Efficiency Sequentially Vapor Grown N-i-p CH3NH3PbI3 Perovskite Solar Cells with Undoped P3HT as p-Type Heterojunction Layer. *APL Mater.* **2015**, *3*, 016105.

(16) Kottokkaran, R.; Gaonkar, H. A.; Abbas, H. A.; Noack, M.; Dalal, V. Performance and Stability of Co-Evaporated Vapor Deposited Perovskite Solar Cells. *J. Mater. Sci. Mater. Electron.* **2019**, *30*, 5487−5494.

(17) Kottokkaran, R.; Gaonkar, H. A.; Bagheri, B.; Dalal, V. L. Efficient p-i-n inorganic CsPbI3 perovskite solar cell deposited using layer-by-layer vacuum deposition. *J. Vac. Sci. Technol., A* **2018**, *36*, 041201.

(18) Conings, B.; Drijkoningen, J.; Gauquelin, N.; Babayigit, A.; D'Haen, J.; D'Olieslaeger, L.; Ethirajan, A.; Verbeeck, J.; Manca, J.; Mosconi, E.; Angelis, F. D.; Boyen, H.-G. Intrinsic Thermal Instability of Methylammonium Lead Trihalide Perovskite. *Adv. Energy Mater.* **2015**, *5*, 1500477.

(19) Kottokkaran, R.; Abbas, H.; Balaji, G.; Liang Zhang, L.; Samiee, M.; Kitahara, A.; Noack, M.; Dalal, V. Highly Reproducible Vapor Deposition Technique, Device Physics and Structural Instability of Perovskite Solar Cells. *2015 IEEE 42nd Photovoltaic Specialist Conference (PVSC)*; IEEE, 2015; pp 1−4.

(20) Cheacharoen, R.; Boyd, C. C.; Burkhard, G. F.; Leijtens, T.; Raiford, J. A.; Bush, K. A.; Bent, S. F.; McGehee, M. D. Encapsulating Perovskite Solar Cells to Withstand Damp Heat and Thermal Cycling. *Sustain. Energy Fuels* **2018**, *2*, 2398−2406.

(21) Dubey, R.; Chattopadhyay, S.; Kuthanazhi, V.; Kottantharayil, A.; Singh Solanki, C.; Arora, B. M.; Narasimhan, K. L.; Vasi, J.; Bora, B.; Singh, Y. K.; Sastry, O. S. Comprehensive study of performance degradation of field-mounted photovoltaic modules in India. *Energy Sci. Eng.* **2017**, *5*, 51−64.

(22) Alonso García, M. C.; Balenzategui, J. L. Estimation of Photovoltaic Module Yearly Temperature and Performance Based on Nominal Operation Cell Temperature Calculations. *Renewable Energy* **2004**, *29*, 1997−2010.

(23) Gaonkar, H.; Zhu, J.; Kottokkaran, R.; Bhageri, B.; Noack, M.; Dalal, V. Thermally Stable, Efficient, Vapor Deposited Inorganic Perovskite Solar Cells. *ACS Appl. Energy Mater.* **2020**, *3*, 3497−3503.

(24) Ma, Q.; Huang, S.; Chen, S.; Zhang, M.; Lau, C. F. J.; Lockrey, M. N.; Mulmudi, H. K.; Shan, Y.; Yao, J.; Zheng, J.; Deng, X.; Catchpole, K.; Green, M. A.; Ho-Baillie, A. W. Y. The Effect of Stoichiometry on the Stability of Inorganic Cesium Lead Mixed-Halide Perovskites Solar Cells. *J. Phys. Chem. C* **2017**, *121*, 19642−19649.

(25) Yuan, H.; Zhao, Y.; Duan, J.; Wang, Y.; Yang, X.; Tang, Q. All-Inorganic CsPbBr3 Perovskite Solar Cell with 10.26% Efficiency by Spectra Engineering. *J. Mater. Chem. A* **2018**, *6*, 24324−24329.

(26) Hua, J.; Deng, X.; Niu, C.; Huang, F.; Peng, Y.; Li, W.; Ku, Z.; Cheng, Y.-b. A Pressure-Assisted Annealing Method for High Quality CsPbBr3 Film Deposited by Sequential Thermal Evaporation. *RSC Adv.* **2020**, *10*, 8905−8909.

(27) Wang, G.; Dong, W.; Gurung, A.; Chen, K.; Wu, F.; He, Q.; Pathak, R.; Qiao, Q. Improving Photovoltaic Performance of Carbon-Based CsPbBr3 Perovskite Solar Cells by Interfacial Engineering Using P3HT Interlayer. *J. Power Sources* **2019**, *432*, 48−54.

(28) Tong, G.; Chen, T.; Li, H.; Qiu, L.; Liu, Z.; Dang, Y.; Song, W.; Ono, L. K.; Jiang, Y.; Qi, Y. Phase Transition Induced Recrystalliza-

tion and Low Surface Potential Barrier Leading to 10.91%-Efficient CsPbBr3 Perovskite Solar Cells. *Nano Energy* **2019**, *65*, 104015.
(29) Li, H.; Tong, G.; Chen, T.; Zhu, H.; Li, G.; Chang, Y.; Wang, L.; Jiang, Y. Interface Engineering Using a Perovskite Derivative Phase for Efficient and Stable CsPbBr3 Solar Cells. *J. Mater. Chem. A* **2018**, *6*, 14255−14261.
(30) Duan, J.; Zhao, Y.; Yang, X.; Wang, Y.; He, B.; Tang, Q. Lanthanide Ions Doped CsPbBr3 Halides for HTM-Free 10.14%-Efficiency Inorganic Perovskite Solar Cell with an Ultrahigh Open-Circuit Voltage of 1.594 V. *Adv. Energy Mater.* **2018**, *8*, 1802346.
(31) Zohar, A.; Kulbak, M.; Levine, I.; Hodes, G.; Kahn, A.; Cahen, D. What Limits the Open-Circuit Voltage of Bromide Perovskite-Based Solar Cells? *ACS Energy Lett.* **2019**, *4*, 1−7.
(32) Xiang, T.; Zhang, Y.; Wu, H.; Li, J.; Yang, L.; Wang, K.; Xia, J.; Deng, Z.; Xiao, J.; Li, W.; Ku, Z.; Huang, F.; Zhong, J.; Peng, Y.; Cheng, Y.-B. Universal Defects Elimination for High Performance Thermally Evaporated CsPbBr3 Perovskite Solar Cells. *Sol. Energy Mater. Sol. Cells* **2020**, *206*, 110317.
(33) Khanal, R.; Ayers, N.; Banerjee, S.; Choudhury, S. Atomic Structure and Electronic Properties of Lead and Tin Based Hybrid Halide Perovskite Surface for Photovoltaic Applications. *AIP Adv.* **2019**, *9*, 085123.
(34) Dalal, V.; Knox, R.; Moradi, B. Measurement of Urbach Edge and Midgap States in Amorphous Silicon P-i-n Devices. *Sol. Energy Mater. Sol. Cells* **1993**, *31*, 349−356.
(35) Kink, R.; Avarmaa, T.; Kisand, V.; Lõhmus, A.; Kink, I.; Martinson, I. Luminescence of cation excitons in and crystals in a wide excitation VUV region. *J. Phys.: Condens. Matter* **1998**, *10*, 693−700.
(36) Li, X.; Tan, Y.; Lai, H.; Li, S.; Chen, Y.; Li, S.; Xu, P.; Yang, J. All-Inorganic CsPbBr3 Perovskite Solar Cells with 10.45% Efficiency by Evaporation-Assisted Deposition and Setting Intermediate Energy Levels. *ACS Appl. Mater. Interfaces* **2019**, *11*, 29746−29752.

https://doi.org/10.1021/acsaem.2c00624
ACS Appl. Energy Mater. 2022, 5, 6265−6273